European Journal of Mechanics B/Fluids 65 (2017) 247–256

Contents lists available at ScienceDirect

European Journal of Mechanics B/Fluids

journal homepage: www.elsevier.com/locate/ejmflu

Explicit solutions for a long-wave model with constant vorticity

Benjamin L. Segal [a], Daulet Moldabayev [b], Henrik Kalisch [b,*], Bernard Deconinck [a]

[a] Department of Applied Mathematics, University of Washington, Seattle, WA 98195-2420, USA
[b] Department of Mathematics, University of Bergen, Postbox 7800, 5020 Bergen, Norway

ARTICLE INFO

Article history:
Received 11 October 2016
Received in revised form
26 February 2017
Accepted 18 April 2017
Available online 6 May 2017

Keywords:
Surface waves
Shear flow
Pressure
Streamlines
Exact solutions

ABSTRACT

Explicit parametric solutions are found for a nonlinear long-wave model describing steady surface waves propagating on an inviscid fluid of finite depth in the presence of a linear shear current. The exact solutions, along with an explicit parametric form of the pressure and streamfunction give a complete description of the shape of the free surface and the flow in the bulk of the fluid. The explicit solutions are compared to numerical approximations previously given in Ali and Kalisch (2013), and to numerical approximations of solutions of the full Euler equations in the same situation Teles da Silva and Peregrine (1988). These comparisons show that the long-wave model yields a fairly accurate approximation of the surface profile as given by the Euler equations up to moderate waveheights. The fluid pressure and the flow underneath the surface are also investigated, and it is found that the long-wave model admits critical layer recirculating flow and non-monotone pressure profiles similar to the flow features of the solutions of the full Euler equations.

1. Introduction

Background vorticity can have a significant effect on the properties of waves at the surface of a fluid [1–10]. In particular, in the seminal paper of Teles da Silva and Peregrine [11], it was found that the combination of strong background vorticity and large amplitude leads to a number of unusual wave shapes, such as narrow and peaked waves and overhanging bulbous waves. In the present contribution, we continue the study of a simplified model equation which admits some of the features found in [11]. The equation, which has its origins in early work of Benjamin [12], has the form

$$\left(Q+\frac{\omega_0}{2}u^2\right)^2\left(\frac{du}{dx}\right)^2 = -3\left(\frac{\omega_0^2}{12}u^4+gu^3-(2R-\omega_0 Q)u^2+2Su-Q^2\right), \tag{1}$$

where we denote the volume flux per unit span by Q, the momentum flux per unit span and unit density corrected for pressure force by S, and the energy density per unit span by R. The gravitational acceleration is g and the constant vorticity is $-\omega_0$. The total flow depth as measured from the free surface to the rigid bottom is given by the function $u(x)$.

Eq. (1) was recently studied in [13]. It was found that solutions of this equation exhibit similar properties as solutions of the full Euler equations displayed in [11]. In particular, in [13] an expression for the pressure was developed, and it was shown that the pressure may become non-monotone in the case of strong background vorticity. Indeed, it was shown in [13] that if $|\omega_0|$ is big enough, the maximum fluid pressure at the bed is not located under the wavecrest. Such behavior is usually only found in transient problems (cf. [14]). Moreover in some cases, the pressure near the crest of the wave may be below atmospheric pressure. In contrast, in an irrotational flow beneath a traveling surface water wave, the pressure is monotone with depth, and no overhanging profiles are possible [15,16].

The purpose of the present work is two-fold. First, we develop a method by which Eq. (1) can be solved *exactly*. The resulting solutions are compared to the numerical approximations found in [13] and to some of the solutions of the full Euler equations from [11]. Secondly, more features of the solutions of (1) are discussed. Using a similar analysis as in [13], the streamfunction is constructed, and it is found that solutions of (1) may feature recirculating flow and pressure inversion. These features may have an impact on the study of sediment resuspension. Indeed, while it is generally accepted that the main mechanism for sediment resuspension is turbulence due to flow separation in the presence of strong viscous shear stresses [17–19], the strongly

* Corresponding author.
E-mail address: henrik.kalisch@math.uib.no (H. Kalisch).

http://dx.doi.org/10.1016/j.euromechflu.2017.04.008
0997-7546/

non-monotone pressure profiles exhibited by the solutions of (1) may represent a more fundamental mechanism for particle suspension than the viscous theory. In particular, in Fig. 13 it can be seen that very strong shear allows for near atmospheric pressure close to the bed, and there are regions of high pressure situated below regions of lower pressure leading to an upwardly directed force in the fluid.

The geometric setup of the problem is explained as follows. Consider a background shear flow $U_0 = \omega_0 z$, where ω can be positive or negative (cf. Fig. 1). Superimposed on this background flow is wave motion at the surface of the fluid. As observed by a number of authors [12,11,9], a linear shear current can be taken as a first approximation of more realistic shear flows with more complex structures.

If it is assumed that the free surface describes a steady periodic oscillatory pattern, then the flow underneath the free surface can be uniquely determined [20–22]. In the presence of vorticity, uniqueness holds under certain conditions, but in some cases, there is loss of uniqueness, and this allows the existence of critical layers in the fluid [23]. For the purpose of studying periodic traveling waves, one may use a reference frame moving with the wave. This change of reference frame leads to a stationary problem in the fundamental domain of one wavelength. The incompressibility guarantees the existence of the streamfunction ψ and if constant vorticity $\omega = -\omega_0$ is stipulated, the streamfunction satisfies the Poisson equation

$$\Delta\psi = \psi_{xx} + \psi_{zz} = \omega_0, \quad \text{in } 0 < z < \eta(x). \tag{2}$$

As explained in [24,25], the three parameters Q, S and R are defined as follows. If $\psi = 0$ on the streamline along the flat bottom, then Q denotes the total volume flux per unit width given by

$$Q = \int_0^\eta \psi_z dz. \tag{3}$$

Thus Q is the value of the streamfunction ψ at the free surface. The flow force per unit width S is defined by

$$S = \int_0^\eta \left\{ \frac{P}{\rho} + \psi_z^2 \right\} dz, \tag{4}$$

and the energy per unit mass is given by

$$R = \frac{1}{2}\psi_z^2 + \frac{1}{2}\psi_x^2 + g\eta \quad \text{on } z = \eta(x). \tag{5}$$

Finally, the pressure can be expressed as

$$P = \rho\Big(R - gz - \frac{1}{2}(\psi_x^2 + \psi_z^2) + \omega_0\psi - \omega_0 Q\Big). \tag{6}$$

It is well known that the quantities Q and S do not depend on the value of x [24]. Using the fact that S is a constant, the derivation of the model equation (1) can be effected by assuming that the waves are long, scaling z by the undisturbed depth h_0, x by a typical wavelength L, and expanding in the small parameter $\beta = h_0^2/L^2$. This yields (1) as an approximate model equation describing the shape of the free surface. In order to distinguish from the free surface η in the full Euler description, we call the unknown of Eq. (1) u which is an approximation of η. The derivation of (1) was given in [24], where it was shown that (1) is expected to be valid as an approximate model equation describing waves on the surface of the shear flow if the wavelength is long compared to the undisturbed depth of the fluid. On the other hand, a detailed analysis of the derivation explained in [24] shows that there are no assumptions on the amplitude of the waves. Thus at least formally, the model (1) can be expected to describe waves of large amplitude.

2. Explicit solutions

In order to obtain solutions of (1) given in explicit form, we apply the change of variables

$$\frac{dy}{ds} = \frac{du}{dx}\left(Q + \frac{\omega_0}{2}u^2\right), \qquad y(s) = u(x).$$

This gives us a new equation for $y(s)$ in the form

$$\left(\frac{dy}{ds}\right)^2 = -3\left(\frac{\omega_0^2}{12}y^4 + gy^3 - (2R - \omega_0 Q)y^2 + 2Sy - Q^2\right), \tag{7}$$

and the relation

$$\frac{ds}{dx} = \frac{1}{Q + y^2\omega_0/2}. \tag{8}$$

Integrating (8) we have

$$x(s) = \int^s \left(Q + \frac{\omega_0}{2}y^2\right) d\xi - x_1 \tag{9}$$

where x_1 is a constant of integration, written explicitly for convenience. We want to solve (7) for $y(s)$ and plug our solution into (9). We notice that in the variables y and $\frac{dy}{ds}$ the equation describes an elliptic curve of genus one [26]. Hermite's Theorem [27, p. 394] states that for a uniform solution to exist we need $\int ds$ to be an abelian integral of the first kind. This condition is indeed satisfied and we proceed with using a birational transformation to put (7) in the standard Weierstraß form

$$\left(\frac{dy_0}{dx_0}\right)^2 = 4y_0^3 - g_2 y_0 - g_3, \tag{10}$$

where the transformation is given in Box I, and g_2 and g_3 are the lattice invariants

$$g_2 = -768QR\omega_0 + 768R^2 - 1152Sg,$$
$$g_3 = 2048Q^3\omega_0^3 - 6144Q^2R\omega_0^2 - 6912Q^2g^2 + 6144QR^2\omega_0 - 4608QSg\omega_0 + 2034S^2\omega_0^2 - 4096R^3 + 9216RSg.$$

It is well known that the solution to (10) is $y_0(x_0) = \wp(x_0 + c_0; g_2, g_3)$, where $\wp$ is the Weierstraß P function and c_0 is an arbitrary constant [28,26]. We invert the birational transformation to determine the exact solution to (7) as

$$y(s) = \frac{A + B\wp'((s+c_0)/4; g_2, g_3) + C\wp((s+c_0)/4; g_2, g_3)}{\wp^2((s+c_0)/4; g_2, g_3) + D\wp((s+c_0)/4; g_2, g_3) + E},$$

with

$$A = -288Q^2g - 96Q\omega_0 S + 192RS, \qquad B = \sqrt{12}Q,$$
$$C = -24S,$$
$$D = 8Q\omega_0 - 16R, \qquad E = 64Q^2\omega_0^2 - 64QR\omega_0 + 64R^2.$$

This gives $u(x(s))$ in the form

$$u(x(s)) = \frac{A + B\wp'((s+c_0)/4; g_2, g_3) + C\wp((s+c_0)/4; g_2, g_3)}{\wp^2((s+c_0)/4; g_2, g_3) + D\wp((s+c_0)/4; g_2, g_3) + E}, \tag{12}$$

as a function of the parameter s. If we express $x(s)$ as a function of s, then we have a parametric representation for $u(x)$, the surface elevation. From (9) we have

$$x(s) = Qs - x_1 + \frac{\omega_0}{2}\int^s y^2(\xi)d\xi. \tag{13}$$

Expanding and simplifying $y(s)^2$ gives

$$y^2 = \frac{4B\wp^3 + C^2\wp^2 + (2AC - B^2g_2)\wp + (A^2 - B^2g_3)}{(\wp^2 + D\wp + E)^2} + \frac{2AB - 2BC\wp}{(\wp^2 + D\wp + E)^2}\wp', \tag{14}$$

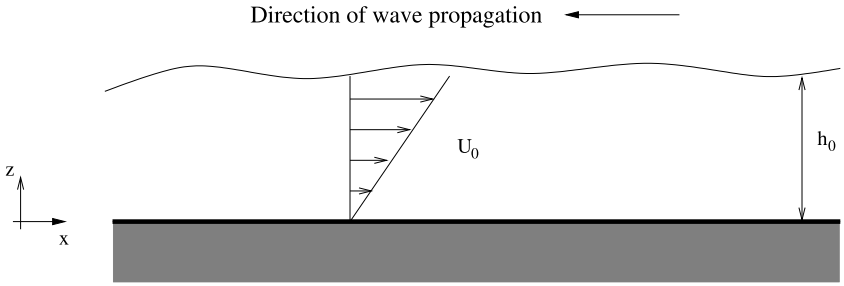

Fig. 1. This figure shows the background shear flow $U_0 = \omega_0 z$. In the figure, ω_0 is positive, and the waves which are superposed onto this background current propagate to the left.

$$x_0 = -\frac{24\left(-2\sqrt{12}Q^2y^2\omega_0 - \sqrt{12}Qgy^3 + 4\sqrt{12}QRy^2 + 4\sqrt{12}Q^3 - 6\sqrt{12}QSy + 8Q^2\frac{dy}{ds} - 4\frac{dy}{ds}Sy\right)}{y^3},$$
$$y_0 = \frac{4\left(-Qy^2\omega_0 + 2Ry^2 + \frac{dy}{ds}\sqrt{12}Q + 6Q^2 - 6Sy\right)}{y^2}, \tag{11}$$

Box I.

making use of the shorthand $\wp = \wp((s+c_0)/4; g_2, g_3)$ and $\wp' = \wp'((s+c_0)/4; g_2, g_3)$. Plugging (14) into (13) and integrating gives

$$x(s) = Qs - x_1 + \omega_0 B\left[\frac{8(2A-CD)\arctan\left(\frac{D+2\wp}{\sqrt{-D^2+4E}}\right)}{(-D^2+4E)^{3/2}} + \frac{-4AD+8CE+(-8A+4CD)\wp}{(D^2-4E)(\wp^2+D\wp+E)}\right] + \frac{\omega_0}{2}\int^s \frac{4B\wp^3 + C^2\wp^2 + (2AC - B^2g_2)\wp + (A^2 - B^2g_3)}{(\wp^2+D\wp+E)^2}d\xi. \tag{15}$$

This integral can be evaluated exactly, and is then written as

$$\begin{aligned} x(s) = {} & Q(s+c_0) - x_2 + \omega_0 B \\ & \times\left[\frac{8(2A-CD)\arctan\left(\frac{D+2\wp}{\sqrt{-D^2+4E}}\right)}{(-D^2+4E)^{3/2}} + \frac{-4AD+8CE+(-8A+4CD)\wp}{(D^2-4E)(\wp^2+D\wp+E)}\right] \\ & + 2\omega_0\big[J(m_1,n_1)I_2((s+c_0)/4,\alpha) + K(m_1,n_1)I_1((s+c_0)/4,\alpha) \\ & + J(n_1,m_1)I_2((s+c_0)/4,\beta) + K(n_1,m_1)I_1((s+c_0)/4,\beta)\big], \end{aligned} \tag{16}$$

where I_1 and I_2 can be found in [28,29], and the functions $J(m_1, n_1)$ and $K(m_1, n_1)$ and the constants m_1 and m_2 are defined in Appendix A.

Thus we have $x(s)$ given in (16) and $u(x(s))$ given in (12) both as functions of s. This gives a parametric representation of our solution as a function of s

$$\begin{cases} y = u(x(s)), & \text{given in (12)}, \\ x = x(s), & \text{given in (16)}. \end{cases} \tag{17}$$

In [13], it was shown how the pressure in the bulk of the fluid can be approximated by the expression

$$\begin{aligned} P = \rho\Bigg\{ & R - gz - \frac{1}{2}\left(\frac{Q}{u^2} + \frac{\omega_0}{2}\right)^2 (z^2u'^2 + u^2) \\ & + \frac{1}{2}\left(\frac{\omega_0}{6}u^3 - \frac{\omega_0}{2}z^2u - \frac{2}{3}\omega_0 z^3 - \frac{Q}{3}u + z^2\frac{Q}{u}\right) \\ & \times\left(2Q\frac{u'^2}{u^3} - u''\left(\frac{Q}{u^2} + \frac{\omega_0}{2}\right)\right)\Bigg\}. \end{aligned} \tag{18}$$

This leads to a parametric representation of the pressure as a function of s and the distance from the channel bed z.

Finally, note that an expression for the streamfunction can be derived using the techniques of [13]. Since this was not done in [13], the derivation is outlined in Appendix B for the sake of completeness. The expression for the streamfunction is

$$\begin{aligned} \psi = {} & \frac{1}{2}z^2\omega_0 + z\left(\frac{Q}{u} - \frac{u\omega_0}{2} + \frac{Qu'^2}{3u} - \frac{Qu''}{6} - \frac{\omega_0 u^2 u''}{12}\right) \\ & - \frac{z^3}{6}\left(\frac{2Qu'^2}{u^3} - \frac{Qu''}{u^2} - \frac{\omega_0 u''}{2}\right), \end{aligned} \tag{19}$$

which gives a parametric representation of the streamfunction as a function of s and z.

3. Matching the explicit solutions to previous works

First, we compare the explicit solutions found here and the numerical approximations given in [13]. Following the analysis of [13], we first note that (1) can be written in the form

$$u'^2 = \frac{\mathcal{G}(u)}{\mathcal{F}(u)}. \tag{20}$$

Letting Z_1, Z_2, m and M represent the roots of the numerator $\mathcal{G}$ on the right-hand side of (20) we write

$$\begin{aligned} \mathcal{G}(u) &= -3\left(\frac{\omega_0^2}{12}u^4 + gu^3 - (2R - \omega_0 Q)u^2 + 2Su - Q^2\right) \\ &= \frac{\omega_0^2}{4}(M-u)(u-m)(u-Z_1)(u-Z_2). \end{aligned} \tag{21}$$

By comparing the coefficients of (21) and assuming that Q, m, and M are given, the two additional roots Z_1 and Z_2 are found as (note that a small typo in [13] has been corrected here)

$$Z_1 = \frac{1}{2}\left\{ -\left(\frac{12}{\omega_0^2}g + (M+m)\right) - \sqrt{\left(\frac{12}{\omega_0^2}g + (M+m)\right)^2 + \frac{48Q^2}{\omega_0^2 mM}}\right\},$$

$$Z_2 = \frac{1}{2}\left\{ -\left(\frac{12}{\omega_0^2}g + (M+m)\right) + \sqrt{\left(\frac{12}{\omega_0^2}g + (M+m)\right)^2 + \frac{48Q^2}{\omega_0^2 mM}}\right\}.$$

The total head R and the flow force S are obtained as

$$R = \frac{\omega_0 Q}{2} - \frac{\omega_0^2}{24}\left(Z_1Z_2 + mM + (M+m)(Z_1+Z_2)\right),$$

$$S = -\frac{\omega_0^2}{24}\left((M+m)Z_1Z_2 + mM(Z_1+Z_2)\right).$$

Following the work in [13] there are two cases depending on the sign of ω_0. If $\omega_0 > 0$, then u'^2 has no singularities and there is a smooth periodic solution if $Z_2 < m < M$. If $\omega_0 < 0$, then u'^2 has two singularities and the parameter space is more restricted. To find the conditions for smooth solutions to exist, we let $\mathcal{F}(u)$ be expressed as

$$\mathcal{F}(u) = \left(Q + \frac{\omega_0}{2}u^2\right)^2 = \frac{\omega_0^2}{4}(u-A_+)^2(u-A_-)^2, \tag{22}$$

which reveals that the derivative is singular when u takes the values $A_+ = \sqrt{\frac{2Q}{-\omega_0}}$ and $A_- = -\sqrt{\frac{2Q}{-\omega_0}}$. In the case $\omega_0 < 0$, smooth solutions exist when $M < A_+$. To better understand this condition, we introduce the non-dimensional Froude number

$$F = \frac{\omega_0 M^2}{2Q}.$$

Substituting F for ω_0 we find four cases:

$$\begin{cases} 0 < F: & \text{smooth solutions exist if } Z_2 < m < M, \\ -1 < F < 0: & \text{smooth solutions exist,} \\ F = -1: & \text{limiting case of smooth solutions ceasing to exist,} \\ F < -1: & \text{no solutions of (1) exist, solutions of (7), (9) are multi-valued.} \end{cases} \tag{23}$$

In [13], only the first two cases above are treated as it is more challenging to compute cusped profiles numerically, and the multi-valued profiles given by the parametric solution of (7), (8) do not correspond to solutions of the model equation (1). Below we show one representative example of each of the cases. As in [13], we use the parameters

$$g = 9.81; \quad \rho = 1; \quad m = 1.1; \quad Q = 1.2\sqrt{g}; \quad h_0 = \sqrt[3]{g^{-1}Q^2}; \quad \omega_0 = \frac{2QF}{M^2}. \tag{24}$$

Additionally, in order to obtain periodic solutions with $m < u(x) < M$ and with zero imaginary part, we need to set

$$c_0 = 4\omega_2(g_2, g_3), \tag{25}$$

where ω_2 is a Weierstraß half period corresponding to the lattice invariants g_2 and g_3 with non-zero imaginary part. Note that since these functions are symmetric under spatial translations (varying x_2) we can shift the waves so they coincide with those in [13]. Indeed this symmetry is inherent to two-dimensional traveling water waves, even in the presence of underlying critical layers [30–32].

Figs. 2 and 3 show two curves found in [13], and no visual difference can be detected between the explicit solutions and the numerical approximations of [13]. We notice that $x(s)$ is a monotone function of s as $F > -1$ decreases up until the critical value of $F = -1$. Beyond the critical point where $F = -1$, $x(s)$ is no longer monotone and as a result the solutions are no longer smooth. Fig. 4 shows the limiting case of a cusped solution, such as also found for the famous Gerstner wave [33]. Note that the evaluation of the pressure at the bottom under the wavecrest appears to yield extremely low and apparently non-physical values. Fig. 5 shows a looped (or self-intersecting) solution which is allowed in Eqs. (7) and (9), but not possible in (1). Since it was assumed in the derivation that the free surface is a single-valued function of x, the solution shown in Fig. 5 is beyond the physical validity of the equation.

Next we investigate whether the solutions of (1) are close to the solutions of the full Euler equations with a background shear flow found in [11]. To facilitate this comparison, we need solutions of (7) (8) which are 2π periodic in x. First, let us examine the periods of $x(s)$ and $u(s)$. Let ω_1 be the Weierstraß half period corresponding to the lattice invariants g_2 and g_3 with non-zero real part. We note that

$$u(s + T_u) = u(s),$$

where

$$T_u = 8\omega_1,$$

denotes the period of $u(x)$, since both $\wp((s+c_0)/4; g_2, g_3)$ and $\wp'((s+c_0)/4; g_2, g_3)$ are periodic of period $8\omega_1$. Next we notice that

$$x(s + T_u) = x(s) + T_x,$$

where

$$T_x = QT_u + 2\omega_0\left[J(m_1,n_1)J_2(\alpha) + K(m_1,n_1)J_1(\alpha) + J(n_1,m_1)J_2(\beta) + K(n_1,m_1)J_1(\beta)\right],$$

with

$$J_1(\gamma) = \frac{1}{\wp'(\gamma)}\left(-4\zeta(\omega_1)\gamma + 4\omega_1\zeta(\gamma)\right),$$

and

$$J_2(\gamma) = \frac{\wp''(\gamma)}{\wp'^3(\gamma)}4\zeta(\omega_1)\gamma - \frac{4\zeta(\omega_1)}{\wp'^2(\gamma)} - 2\omega_1\left(\frac{2\wp(\gamma)}{\wp'^2(\gamma)} + \frac{2\wp''(\gamma)\zeta(\gamma)}{\wp'^3(\gamma)}\right).$$

This was determined by noting that

$$I_1(u + 2\omega_1, \gamma) = I_1(u,\gamma) + J_1(\gamma),$$
$$I_2(u + 2\omega_1, \gamma) = I_2(u,\gamma) + J_2(\gamma),$$

which we see from [34]:

$$\zeta(u + 2\omega_1) = \zeta(z) + 2\zeta(\omega_1),$$
$$\sigma(u + 2\omega_1) = -e^{2\zeta(\omega_1)(u+\omega_1)}\sigma(z).$$

Now since T_x gives an analytical expression for the wavelength of the solution, using the scaling symmetry of (1), and rescale x by $2\pi/T_x$ and u by $2\pi/T_x$ will yield 2π-periodic solutions.

For the sake of completeness, let us also describe how to shift the wave profiles in the parametric representation in order to locate the peak of the wave at a given point, say $x = 0$. To achieve

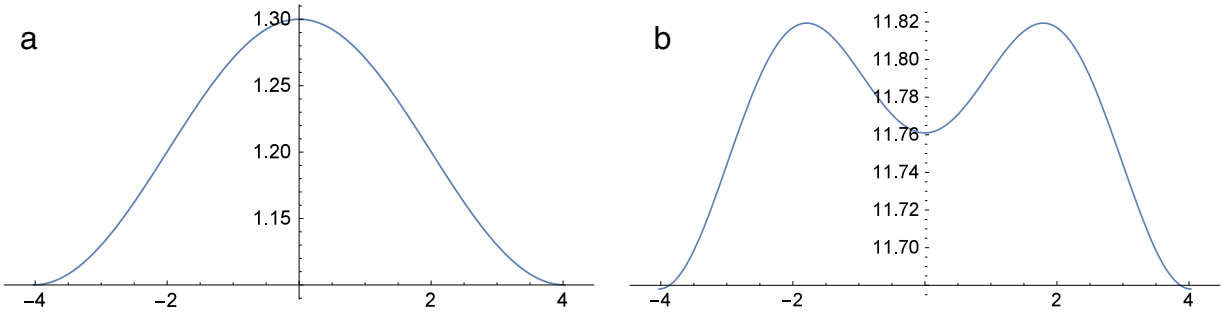

Fig. 2. Solution of (7), (8) in the case $F = 1.15, M = 1.3$, plotted for $-\frac{1}{2} \le s \le \frac{1}{2}$. (a) Surface profile $u(x)$ as a function of x. (b) Bottom pressure $P(u(x), 0)$ as a function of x.

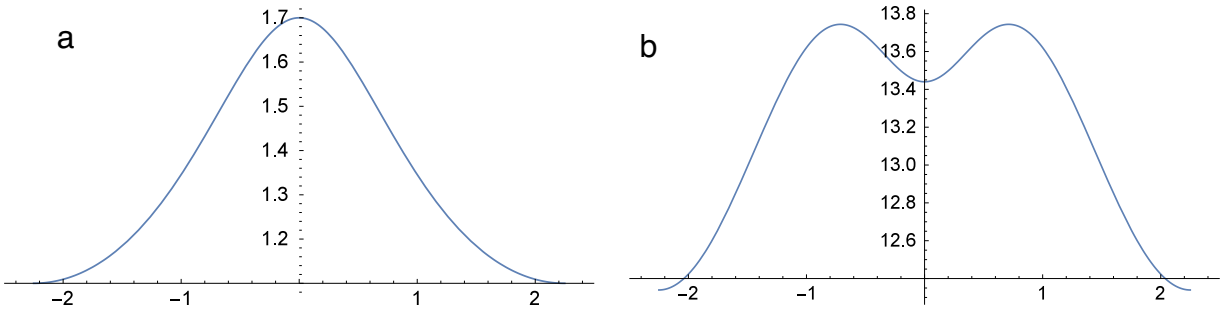

Fig. 3. Solution of (7), (8) in the case $F = -0.3, M = 1.7$, plotted for $-\frac{1}{2} \le s \le \frac{1}{2}$. (a) Surface profile $u(x)$ as a function of x. (b) Bottom pressure $P(u(x), 0)$ as a function of x.

this we determine the value of s for which $u(s)$ is at a peak and call this value T_s. Taking (11) we have

$$\wp((T_s + c_0)/4, g_2, g_3) = \frac{4(-QM^2\omega_0 + 2RM^2 + 6Q^2 - 6SM)}{M^2},$$

where we plugged in $y = M$ and $dy/ds = 0$ to be at the peak of the wave. This gives

$$T_s = 4\wp^{-1}\left(\frac{4(-QM^2\omega_0 + 2RM^2 + 6Q^2 - 6SM)}{M^2}, g_2, g_3\right) - c_0.$$

Thus for solutions with the peak at $x = 0$, we rewrite (17) as

$$\begin{cases} y = u(T_u(s - T_s)), & \text{given in (12)}, \\ x = x(T_u(s - T_s)), & \text{given in (16)}. \end{cases} \tag{26}$$

Additionally, we set

$$\begin{aligned} x_2 = T_u \Bigg(& Q(\tilde{s} + c_0) + \omega_0 B \\ & \times \Bigg[\frac{8(2A - CD)\arctan\left(\frac{D + 2\wp((\tilde{s}+c_0)/4)}{\sqrt{-D^2+4E}}\right)}{(-D^2 + 4E)^{3/2}} \\ & + \frac{-4AD + 8CE + (-8A + 4CD)\wp((\tilde{s} + c_0)/4)}{(D^2 - 4E)(\wp((\tilde{s} + c_0)/4)^2 + D\wp((\tilde{s} + c_0)/4) + E)} \Bigg] \\ & + 2\omega_0 \big[J(m_1, n_1) I_2((\tilde{s} + c_0)/4, \alpha) \\ & + K(m_1, n_1) I_1((\tilde{s} + c_0)/4, \alpha) \\ & + J(n_1, m_1) I_2((\tilde{s} + c_0)/4, \beta) \\ & + K(n_1, m_1) I_1((\tilde{s} + c_0)/4, \beta) \big] \Bigg), \end{aligned} \tag{27}$$

where $\tilde{s} = T_u(0 - T_s)$. This x_2 is chosen so that when $s = 0$, $x = 0$. Additionally, note that we scale s by T_u. The scaling of s is so that as s ranges from $-1/2$ to $1/2$, we plot exactly one period of wavelength T_x.

We compare some wave profiles presented in Fig. 6 of by Teles da Silva and Peregrine [11] with solutions of same parameters computed by the current explicit method. Note that in [11], the parameters g and h_0 were normalized, so that we need to choose $g = 1$ and $h_0 = 1$. We first present a comparison of a traveling wave of waveheight $H = 1$ and vorticity $\omega_0 = -3$. In order to get a good match with the plot from Fig. 6 of [11], we selected $m = 1.44, M = 2.44, Q = 0.09$. Fig. 6 shows an explicit solution of (1) compared to a solution of the full Euler equations shown in Fig. 6 in [11]. Even though the waveheight–depth ratio of $1/2$ is not very small, the profiles match fairly closely.

Comparing higher-amplitude waves is more difficult since the solutions shown in [11] with waveheight larger than 1 are overhanging. Setting all parameters correctly yields the comparison shown in Fig. 7. As can be seen, the wavelength matches, and the parametric solutions of (7), (9) are also overhanging, but look very different nevertheless. One may conclude from this last comparison, that if solutions of (7), (9) are not single-valued, and therefore are beyond the validity of (1), they will not in general represent the physical reality of the surface-water wave problem.

4. Pressure contours and streamlines

In this section, we explore the flow underneath the surface as predicted by (1), with the help of the expression (18) for the pressure and (19) for the streamfunction. We should mention that there are a number of works which discuss the flow field underneath surface waves in the context of model equation. In particular, in [35], the velocity field corresponding to cnoidal surface profiles is constructed. In [36] the streamlines of the flow associated to the KdV model are constructed, and in [37], particle trajectories corresponding to KdV surface profiles are found. While these works all focus on the irrotational case, the present study

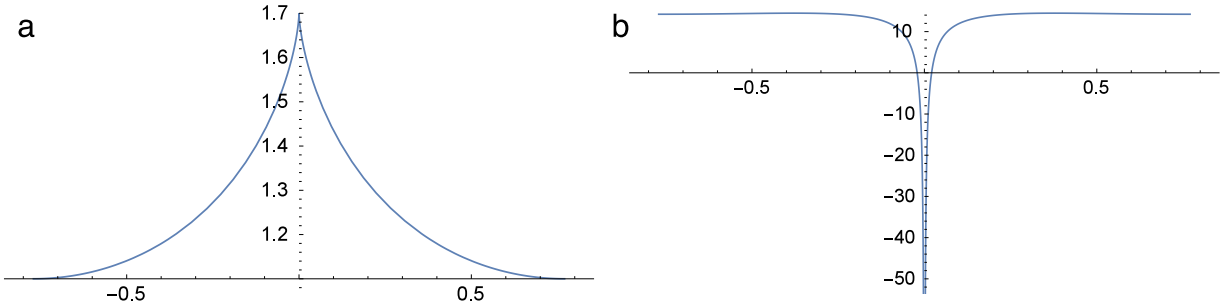

Fig. 4. Solution of (7), (8) in the limiting case $F = -1$, with $M = 1.7$, plotted for $-\frac{1}{2} \le s \le \frac{1}{2}$. (a) Surface profile $u(x)$ as a function of x is cusp-shaped. (b) Bottom pressure appears non-physical.

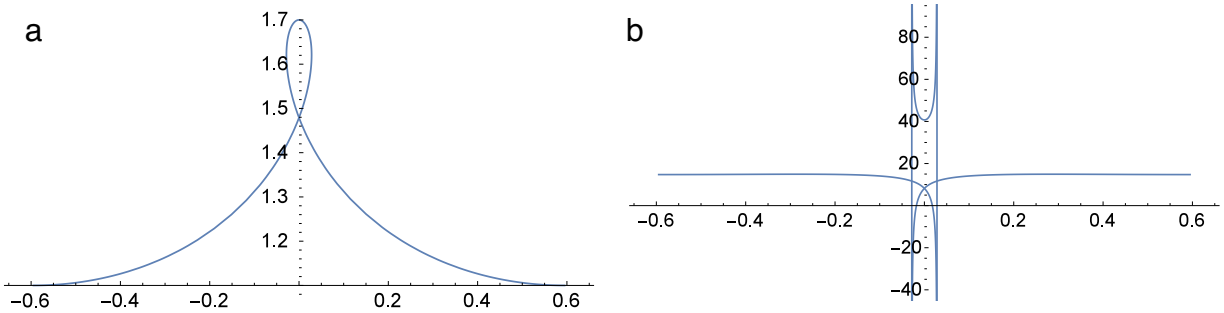

Fig. 5. Solution of (7), (8) in the case $F = -1.1$, with $M = 1.7$. (a) Plotting $u(x)$ as a function of x yields multi-valued profile which is not a solution of (1). (b) Bottom pressure clearly non-physical.

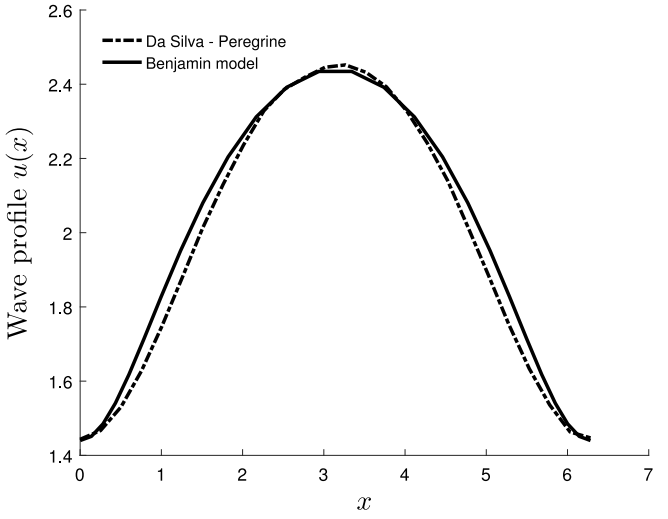

Fig. 6. Comparing approximate solutions of the full Euler equations (dashed curve) to exact solutions of (1) (solid curve). The waves have waveheight $H = 1$ and wavelength 2π. The problem is normalized with $g = 1$ and $h_0 = 1$, and the background vorticity is $\omega_0 = -3$.

explicitly incorporates background vorticity into the model as explained in the derivation of (1).

First, pressure contours and streamlines are reviewed for positive Froude numbers F. This case corresponds to the case labeled 'upstream' in [11]. As mentioned in that work, it is in this case that a critical layer is possible. Examining Figs. 8–13, it appears that as the strength of the vorticity increases, first, the pressure becomes non-monotone (Fig. 9). In other words, the pressure strongly departs from hydrostatic pressure, the bottom pressure is maximal under the sides of the wave (not the crest), and this goes hand in hand with the development of closed streamlines (Fig. 10). For large enough Froude numbers, a critical layer (i.e., a closed circulation) develops in the interior of the fluid domain (Fig. 11). In the extreme case of $F = 3$, pressure inversion occurs as regions of high pressure are above regions of low pressure in the fluid column (Fig. 13).

For negative Froude numbers, the flow corresponds to the downstream case [11]. Figs. 14 and 15 show pressure contours and streamlines for low values of the Froude number. For larger Froude numbers, non-monotone pressures develop also in this case, but no critical layer occurs in the fluid domain. Figs. 16 and 17 show strongly non-monotone pressures. Apparently, as the shape of the free surface approaches a cusped profile, non-physical features appear in the description of the flow.

5. Conclusion

The nonlinear differential equation (1) is known to be a model for steady surface water waves on a background shear flow. The equation has been found to admit solutions given explicitly in terms of a parametric representation featuring the Weierstraß P, zeta and sigma functions. This representation is a convenient tool for obtaining a variety of wave profiles without having to resort to numerical approximation. In connection with the reconstruction of the pressure underneath the surface explained in [13], and the reconstruction of the streamfunction detailed in the Appendix, a complete description of the flow can be obtained.

The exact solutions of (1) have been compared to wave profiles obtained from full Euler computations in [11], and fair agreement was found for regular waves. On the other hand, overhanging waves were found not to agree with the full Euler solutions. This is not surprising since the parametric representation enables the description of multi-valued profiles which transcends the collection of solutions of (1).

With a view towards the flow in the fluid column below the wave, a number of wave shapes with increasing strength of vorticity were exhibited. It was found in the case of steady waves propagating upstream that the flow underneath the waves may feature critical layers and non-monotone pressure profiles. In

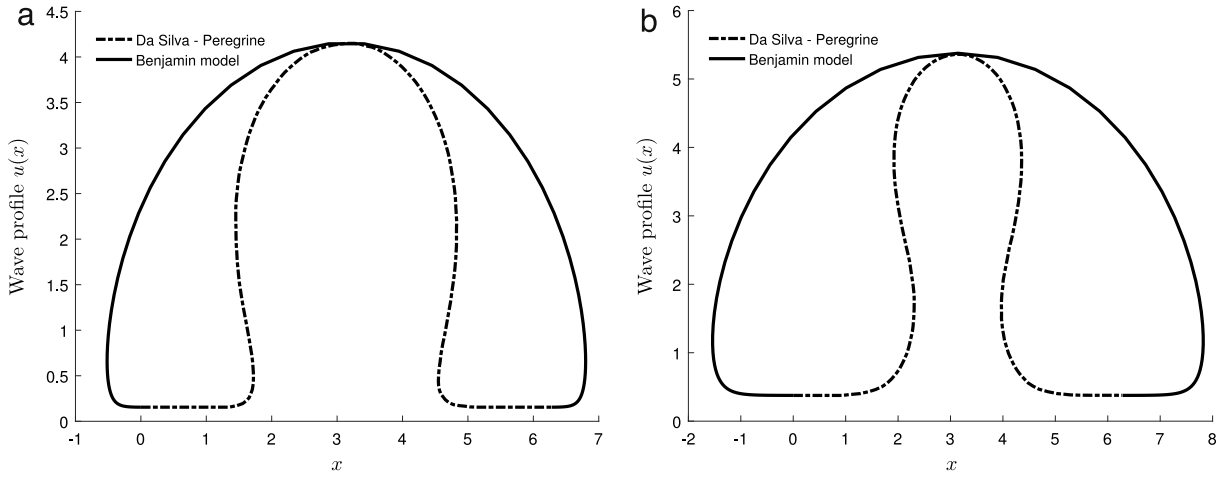

Fig. 7. Comparing approximate solutions of the full Euler equations (dashed curve) to exact solutions of (8), (9) (solid curve). The problem is normalized with $g = 1, h_0 = 1$ and wavelength 2π. The background vorticity is $\omega_0 = -3$. (a) Waveheight $H = 4$. (b) Waveheight $H = 5$.

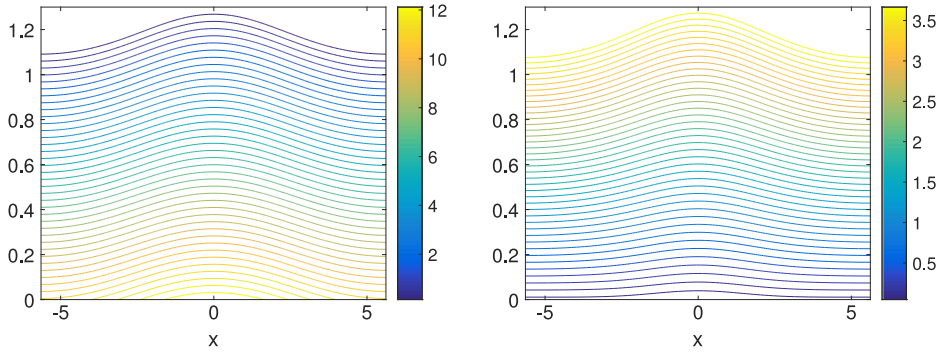

Fig. 8. Traveling wave with $m = 1.1$, $M = 1.3$, and $F = 0.2$. Left: pressure contours. Right: streamlines.

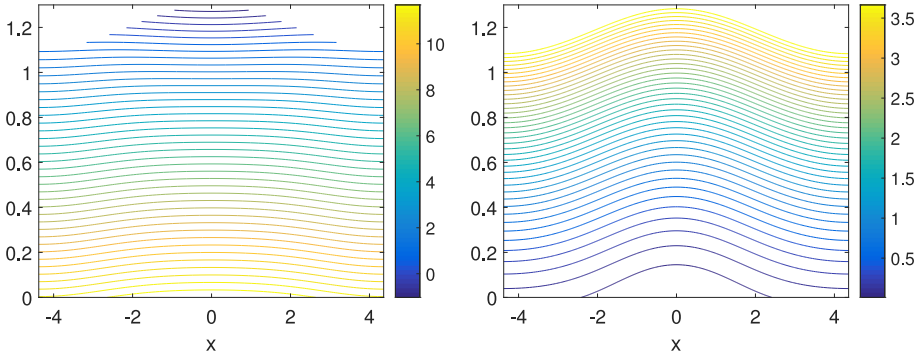

Fig. 9. Traveling wave with $m = 1.1$, $M = 1.3$, and $F = 0.9$. Left: pressure contours. Right: streamlines.

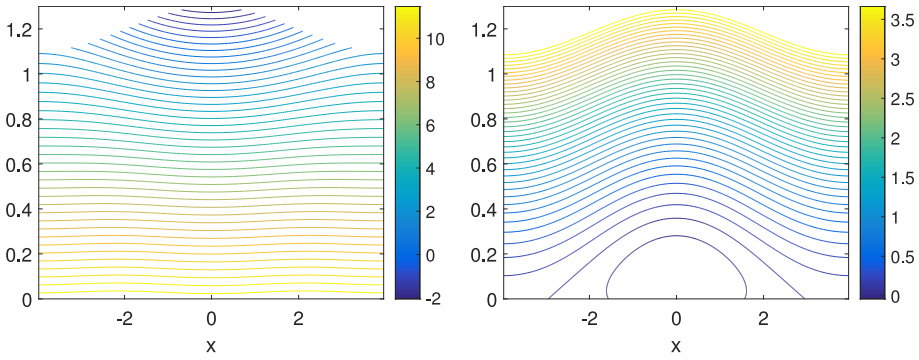

Fig. 10. Traveling wave with $m = 1.1$, $M = 1.3$, and $F = 1.2$. Left: pressure contours. Right: streamlines.

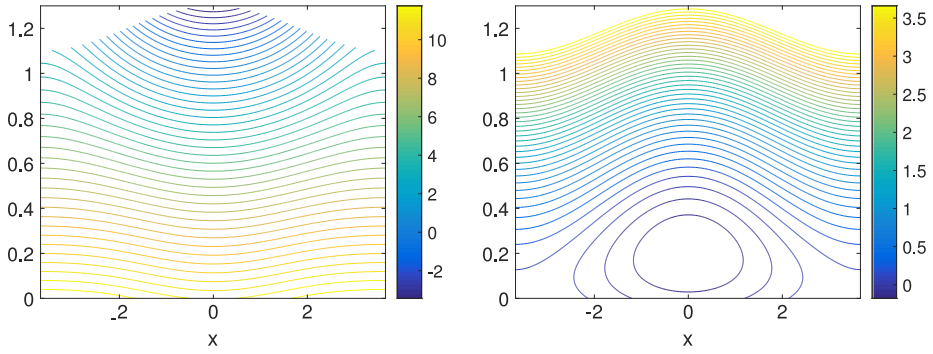

Fig. 11. Traveling wave with $m = 1.1$, $M = 1.3$, and $F = 1.5$. Left: pressure contours. Right: streamlines. Pressure highly non-monotone, critical layer appears.

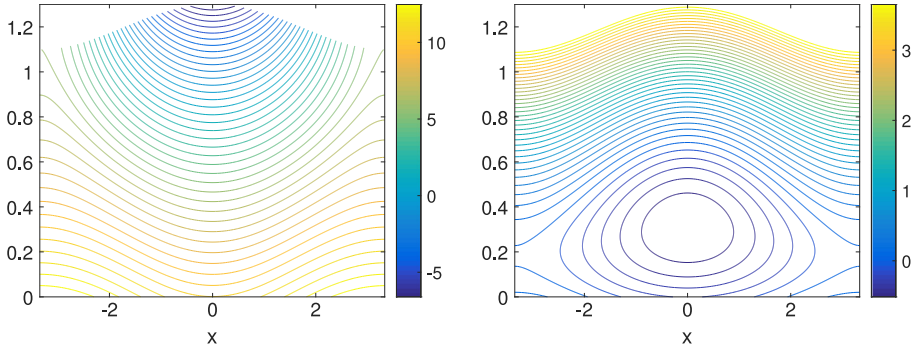

Fig. 12. Traveling wave with $m = 1.1$, $M = 1.3$, and $F = 2.0$. Left: pressure contours. Right: streamlines.

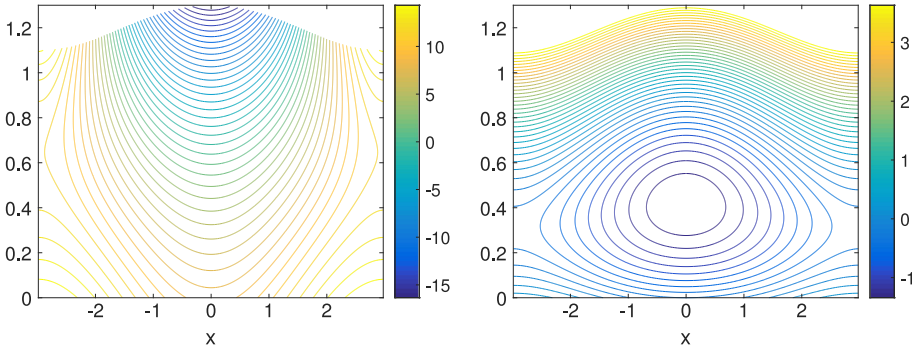

Fig. 13. Traveling wave with $m = 1.1$, $M = 1.3$, and $F = 3.0$. Left: pressure contours. Right: streamlines. Pressure inversion: high pressure above low pressure.

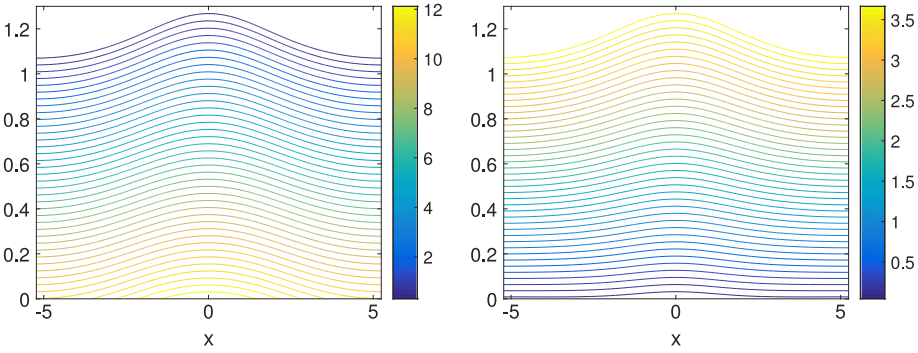

Fig. 14. Traveling wave with $m = 1.1$, $M = 1.3$, and $F = -0.001$. Left: pressure contours. Right: streamlines.

the case of waves propagating downstream, the development of cusped surface profiles goes hand in hand with unrealistic pressure profiles apparently conflicting with the long-wave approximation which is the basis for the model (1). Building on the results of this paper, future work may focus on detailed comparisons of the fluid flow as described by the methods of the current work to numerical approximations of the flow governed by the Euler equations with background vorticity. Such a study will cast more light on the

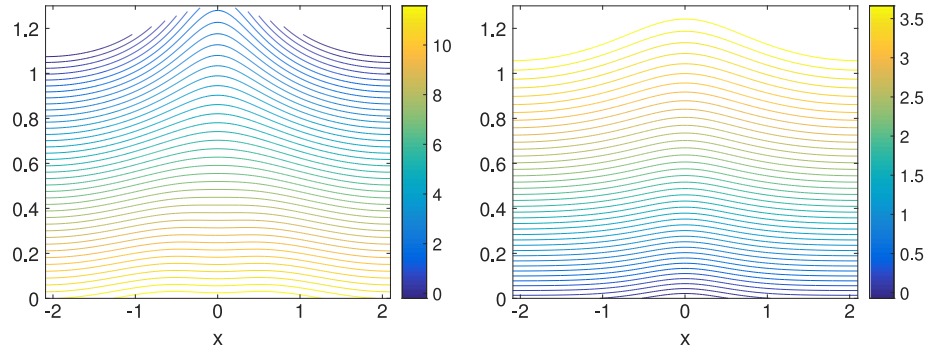

Fig. 15. Traveling wave with $m = 1.1$, $M = 1.3$, and $F = -0.5$. Left: pressure contours. Right: streamlines.

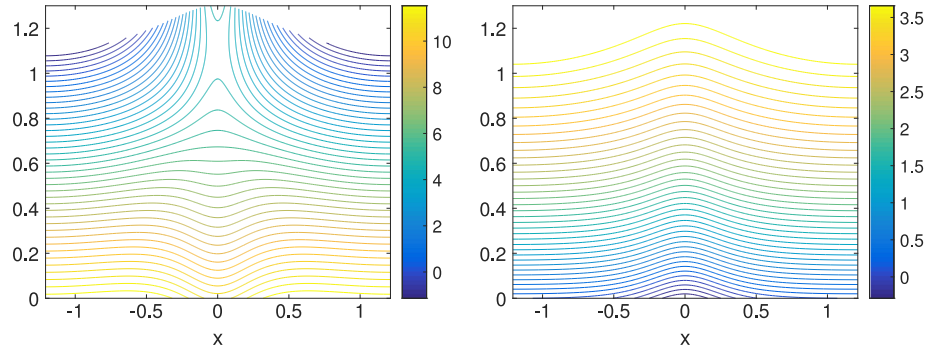

Fig. 16. Traveling wave with $m = 1.1$, $M = 1.3$, and $F = -0.7$. Left: pressure contours. Right: streamlines.

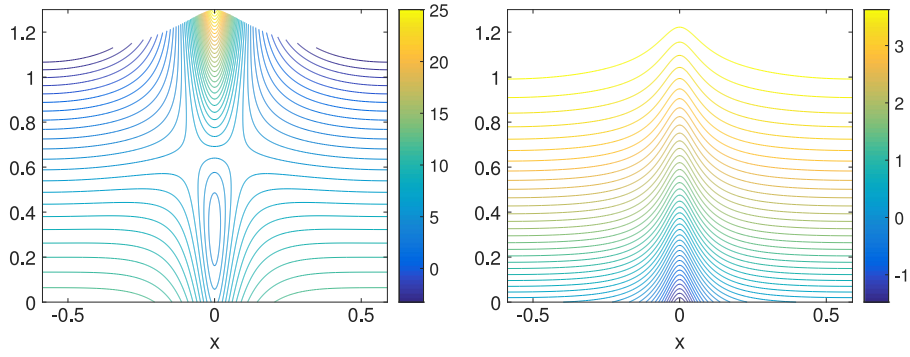

Fig. 17. Traveling wave with $m = 1.1$, $M = 1.3$, and $F = -0.9$. Left: pressure contours. Right: streamlines.

limitations of the current model, especially as regarding the ability to describe properties of the flow in the bulk of the fluid.

Acknowledgments

This research was supported in part by the Research Council of Norway under grant 213474/F20 and by the National Science Foundation under grant NSF-DMS-1008001. Any opinions, findings, and conclusions or recommendations expressed in this material are those of the authors and do not necessarily reflect the views of the funding sources.

Appendix A. Exact evaluation of the integral (15)

To evaluate the integral in (15) we let

$$m_1 = -\frac{D}{2} - \frac{\sqrt{D^2 - 4E}}{2}, \quad \text{and} \quad n_1 = -\frac{D}{2} + \frac{\sqrt{D^2 - 4E}}{2},$$

denote the roots of $\wp^2 + D\wp + E = 0$. Letting

$$\alpha = \wp^{-1}(m_1), \qquad \beta = \wp^{-1}(n_1), \quad \text{and} \quad x_1 = -c_0 Q + x_2,$$

where x_2 is another arbitrary constant, we express $x(s)$ as (16), where the following unnumbered equations given in Box II. ζ is the Weierstraß zeta function and σ is the Weierstraß sigma function.

Appendix B. Reconstruction of the streamfunction

We want to reconstruct the streamfunction $\psi(x, z)$ using the solutions u of the differential equation (1). This is done by using the ansatz

$$\psi = \frac{1}{2}z^2\omega_0 + zf - \frac{1}{3!}z^3 f'', \tag{28}$$

for the streamfunction and the identity

$$Q = \frac{1}{2}u^2\omega_0 + \zeta f - u^3\frac{1}{6}f'',$$

both of which are valid to second order in the long-wave parameter $\beta = h_0^2/\lambda^2$, where h_0 is the undisturbed depth of the fluid, and λ is the wavelength. To obtain an expression for f in terms of ζ, one

$$I_1(u,\gamma) = \frac{1}{\wp'(\gamma)}\left[\log\left(\frac{\sigma(u-\gamma)}{\sigma(u+\gamma)}\right) + 2u\zeta(\gamma)\right],$$
$$I_2(u,\gamma) = \frac{\wp''(\gamma)}{\wp'^3(\gamma)}\log\left(\frac{\sigma(u+\gamma)}{\sigma(u-\gamma)}\right) - \frac{1}{\wp'^2(\gamma)}\left(\zeta(u+\gamma)+\zeta(u-\gamma)\right) - \left(\frac{2\wp(\gamma)}{\wp'^2(\gamma)} + \frac{2\wp''(\gamma)\zeta(\gamma)}{\wp'^3(\gamma)}\right)u,$$
$$J(m_1,n_1) = \frac{A^2 - B^2g_3 + 2ACm_1 - B^2g_2m_1 + C^2m_1^2 + 4B^2m_1^3}{D^2-4E},$$
$$K(m_1,n_1) = \frac{-2A^2 + 2B^2g_3 - 2ACm_1 + B^2g_2m_1 + 4B^2m_1^3 - 2ACn_1 + B^2g_2n_1 - 2C^2m_1n_1 - 12B^2m_1^2n_1}{(4E-D^2)^{3/2}},$$

Box II.

has to invert the operator $1 - \frac{1}{6}\zeta^2\partial_{xx}$, leading to

$$\left[1 - \frac{1}{6}\zeta^2\partial_{xx}\right]^{-1}\left(\frac{Q}{\zeta} - \frac{1}{2}\zeta\omega_0\right) = f.$$

In order to bring out the difference in scales between the undisturbed depth h_0 and the wavelength L, we use the scaling $\tilde{x} = \frac{x}{L}$, $\tilde{z} = \frac{z}{h_0}$, $\tilde{\zeta} = \frac{\zeta}{h_0}$, $\tilde{\psi} = \frac{1}{c_0h_0}\psi$, $\tilde{\omega}_0 = \frac{h_0}{c_0}\omega_0$, In addition, Q is scaled as $\tilde{Q} = \frac{Q}{h_0c_0}$. In non-dimensional variables, the expression for ψ is

$$\tilde{\psi} = \frac{1}{2}\tilde{z}^2\tilde{\omega}_0 + \tilde{z}\tilde{f} - \frac{\beta}{3!}\tilde{z}^3\tilde{f}'' + \mathcal{O}(\beta^2).$$

The function $\tilde{f}$ is written as

$$\tilde{f} = \left[1 + \frac{\beta}{6}\tilde{u}^2\partial_{\tilde{x}}^2 + \mathcal{O}(\beta^2)\right]\left(\frac{\tilde{Q}}{\tilde{u}} - \frac{1}{2}\tilde{u}\omega_0\right) + \mathcal{O}(\beta^2).$$
$$= \frac{\tilde{Q}}{\tilde{u}} - \frac{1}{2}\tilde{u}\tilde{\omega}_0 + \frac{\beta}{3}Q\frac{(\tilde{u}')^2}{\tilde{u}} - \frac{\beta}{6}Q\tilde{u}'' - \frac{\beta}{12}\omega_0\tilde{u}^2\tilde{u}'' + \mathcal{O}(\beta^2).$$

The second derivative is

$$\tilde{f}'' = 2\frac{\tilde{Q}}{\tilde{u}^3}(\tilde{u}')^2 - \frac{\tilde{Q}}{\tilde{u}^2}\tilde{u}'' - \frac{1}{2}\omega_0\tilde{u}'' + \mathcal{O}(\beta).$$

Putting these together, we find the streamfunction in terms of $\tilde{u}$:

$$\tilde{\psi} = \frac{1}{2}\tilde{z}^2\tilde{\omega}_0 + \tilde{z}\left[\frac{\tilde{Q}}{\tilde{u}} - \frac{1}{2}\tilde{u}\tilde{\omega}_0 + \frac{\beta}{3}Q\frac{(\tilde{u}')^2}{\tilde{u}} - \frac{\beta}{6}Q\tilde{u}'' - \frac{\beta}{12}\omega_0\tilde{u}^2\tilde{u}''\right] - \frac{\beta}{3!}\tilde{z}^3\left[2\frac{Q}{\tilde{u}^3}(\tilde{u}')^2 - \frac{Q}{\tilde{u}^2}\tilde{u}'' - \frac{\omega_0}{2}\tilde{u}''\right] + \mathcal{O}(\beta^2).$$

References

[1] A. Constantin, K. Kalimeris, O. Scherzer, Approximations of steady periodic water waves in flows with constant vorticity, Nonlinear Anal. RWA 25 (2015) 276–306.
[2] A. Constantin, K. Kalimeris, O. Scherzer, A penalization method for calculating the flow beneath traveling water waves of large amplitude, SIAM J. Appl. Math. 75 (2015) 1513–1535.
[3] M. Ehrnström, G. Villari, Linear water waves with vorticity: rotational features and particle paths, J. Differential Equations 244 (2008) 1888–1909.
[4] V.M. Hur, Exact solitary water waves with vorticity, Arch. Ration. Mech. Anal. 188 (2008) 213–244.
[5] J. Ko, W. Strauss, Large-amplitude steady rotational water waves, Eur. J. Mech. B Fluids 27 (2008) 96–109.
[6] J. Ko, W. Strauss, Effect of vorticity on steady water waves, J. Fluid Mech. 608 (2008) 197–215.
[7] Y. Li, S.Å. Ellingsen, Ship waves on uniform shear current at finite depth: wave resistance and critical velocity, J. Fluid Mech. 791 (2016) 539–567.
[8] R. Thomas, C. Kharif, M. Manna, A nonlinear Schrödinger equation for water waves on finite depth with constant vorticity, Phys. Fluids 24 (2012) 127102.
[9] J. Touboul, J. Charland, V. Rey, K. Belibassakis, Extended mild-slope equation for surface waves interacting with a vertically sheared current, Coast. Eng. 116 (2016) 77–88.
[10] J.-M. Vanden-Broeck, Periodic waves with constant vorticity in water of infinite depth, IMA J. Appl. Math. 56 (1996) 207–217.
[11] A.F. Teles da Silva, D.H. Peregrine, Steep, steady surface waves on water of finite depth with constant vorticity, J. Fluid Mech. 195 (1988) 281–302.
[12] T.B. Benjamin, The solitary wave on a stream with an arbitrary distribution of vorticity, J. Fluid Mech. 12 (1962) 97–116.
[13] A. Ali, H. Kalisch, Reconstruction of the pressure in long-wave models with constant vorticity, Eur. J. Mech. B Fluids 37 (2013) 187–194.
[14] J. Touboul, E. Pelinovsky, Bottom pressure distribution under a solitonic wave reflecting on a vertical wall, Eur. J. Mech. B Fluids 48 (2014) 13–18.
[15] A. Constantin, W. Strauss, Pressure beneath a Stokes wave, Comm. Pure Appl. Math. 63 (2010) 533–557.
[16] E. Varvaruca, Bernoulli free-boundary problems in strip-like domains and a property of permanent waves on water of finite depth, Proc. Roy. Soc. Edinburgh Sect. A 138 (2008) 1345–1362.
[17] T.L. Clarke, B. Lesht, R.A. Young, D.J.P. Swift, G.L. Freeland, Sediment resuspension by surface-wave action: An examination of possible mechanisms, Mar. Geol. 49 (1982) 43–59.
[18] C.C. Mei, S.-J. Fan, K.-R. Jin, Resuspension and transport of fine sediments by waves, J. Geophys. Res.: Oceans 102 (1997) 15807–15821.
[19] J.S. Ribberink, A.A. Al-Salem, Sediment transport in oscillatory boundary layers in cases of rippled beds and sheet flow, J. Geophys. Res.: Oceans 99 (1994) 12707–12727.
[20] A. Constantin, W. Strauss, Exact steady periodic water waves with vorticity, Comm. Pure Appl. Math. 57 (2004) 481–527.
[21] H. Kalisch, A uniqueness result for periodic traveling waves in water of finite depth, Nonlinear Anal. 58 (2004) 779–785.
[22] A. Constantin, E. Varvaruca, Steady periodic water waves with constant vorticity: regularity and local bifurcation, Arch. Ration. Mech. Anal. 199 (2011) 33–67.
[23] E. Wahlén, Steady water waves with a critical layer, J. Differential Equations 246 (2009) 2468–2483.
[24] T.B. Benjamin, M.J. Lighthill, On cnoidal waves and bores, Proc. Roy. Soc. London Ser. A 224 (1954) 448–460.
[25] A. Ali, H. Kalisch, On the formulation of mass, momentum and energy conservation in the KdV equation, Acta Appl. Math. 133 (2014) 113–131.
[26] R. Conte, M. Musette, The Painlevé Handbook, Springer Science & Business Media, 2008.
[27] G. Valiron, J. Glazebrook, The Geometric Theory of Ordinary Differential Equations and Algebraic Functions, Math Sci Press, 1984.
[28] P.F. Byrd, M.D. Friedman, Handbook of Elliptic Integrals for Engineers and Scientists, Vol. 67, Springer, Berlin, 1971.
[29] I. Gradshteyn, I. Ryzhik, Table of Integrals, Series and Products, fifth ed., Academic Press, New York, 1994.
[30] A. Constantin, M. Ehrnström, E. Wahlén, Symmetry of steady periodic gravity water waves with vorticity, Duke Math. J. 140 (2007) 591–603.
[31] A. Constantin, J. Escher, Symmetry of steady periodic surface water waves with vorticity, J. Fluid Mech. 498 (2004) 171–181.
[32] G. Tulzer, On the symmetry of steady periodic water waves with stagnation points, Commun. Pure Appl. Anal. 11 (2012) 1577–1586.
[33] F. Gerstner, Theorie der Wellen samt der daraus abgeleiteten Theorie der Deichprofile, Ann. Phys. 2 (1809) 412–445.
[34] F.W.J. Olver, D.W. Lozier, D.F. Boisvert, C.W. Clark (Eds.), NIST Handbook of Mathematical Functions, Cambridge University Press, New York, 2010.
[35] D. Clamond, Steady finite-amplitude waves on a horizontal seabed of arbitrary depth, J. Fluid Mech. 398 (1999) 45–60.
[36] D. Henry, Steady periodic flow induced by the Korteweg-de Vries equation, Wave Motion 46 (2009) 403–411.
[37] H. Borluk, H. Kalisch, Particle dynamics in the KdV approximation, Wave Motion 49 (2012) 691–709.